

# Design of Wide-Field Imaging Shack Hartmann Testbed

Lauren H. Schatz, R. Phillip Scott, Ryan S. Bronson, Lucas R.W. Sanchez, and Michael Hart  
College of Optical Sciences, University of Arizona, 1630 E University Blvd, Tucson, AZ, 85721,  
USA

## ABSTRACT

Standard adaptive optics systems measure the aberrations in the wavefronts of a beacon guide star caused by atmospheric turbulence, which limits the corrected field of view to the isoplanatic patch, the solid angle over which the optical aberration is roughly constant. For imaging systems that require a corrected field of view larger than the isoplanatic angle, a three-dimensional estimate of the aberration is required. We are developing a wide-field imaging Shack-Hartmann wavefront sensor (WFS) that will characterize turbulence over a large field of view tens of times the size of the isoplanatic angle. The technique will find application in horizontal and downward looking remote sensing scenarios where high resolution imaging through extended atmospheric turbulence is required. The laboratory prototype system consists of a scene generator, turbulence simulator, a Shack Hartman WFS arm, and an imaging arm. The system has a high intrinsic Strehl ratio, is telecentric, and diffraction limited. We present preliminary data and analysis from the system.

**Keywords:** Wavefront Sensor, Aberrations, Turbulence, Imaging, Shack Hartmann

## 1. INTRODUCTION

Atmospheric turbulence affects all terrestrial imaging systems, severely degrading the resolution of images. Standard single-conjugate adaptive optics (AO) systems measure the aberrations in the wave-fronts of beacon guide stars, then calculate and apply the corrections via an adaptive mirror, which limits the corrected field of view to the isoplanatic angle. Such systems have great value in astronomy and laser communication systems where a narrow field of view does not necessarily compromise utility. However, imaging systems for terrestrial remote sensing generally require a corrected field of view many times larger than the isoplanatic angle. Correcting the image along many lines of sight simultaneously requires the characterization of the aberrations in three dimensions.

Building on the concept of the imaging Shack-Hartmann sensor pioneered in wide-field AO for solar astronomy,<sup>1,2</sup> we have shown in simulation that the technique holds promise for wide-field imaging scenarios. As used in solar multi-conjugate adaptive optics (MCAO) systems, small regions of the image containing high contrast, high spatial frequency information replace guide stars as the reference beacons for the 3D reconstruction of aberrations. The full scene is projected through each of the sensor's sub-apertures to form a set of images. Each image is divided into contiguous regions the size of the isoplanatic patch that are cross-correlated to the corresponding regions in a reference image. The position of each cross-correlation peak is a measure of the line-of-sight wave-front phase gradient between the point in the scene represented by the image region and the point in the pupil represented by the sub-aperture. This concept is shown in Figure 1. As shown in Figure 2 these relative shifts of the features can be represented as a warp map which characterizes the spatial gradient of the aberration across the scene. A 3D reconstruction of the wave-front gradients is recovered via tomosynthesis from the warp maps of all the sub-apertures.<sup>3</sup> The aberrations then can either be directly removed by driving a set of deformable mirrors conjugated to appropriate ranges within the bulk turbulence, or used to compute point-spread functions (PSFs) as a function of position within the field that may be numerically removed from the image to restore high resolution.

We have built a simulation of the technique in MATLAB. The modeled geometry is a scene at 25 km range observed through a 20 cm telescope along a near-horizontal down-slant path over a 400  $\mu$ rad field of view (FOV). Two dynamic Kolmogorov aberration layers warp the scene, one in the pupil plane of the telescope with a spatial coherence length  $r_0$  of 2.7 cm, and one at 3300 m range with  $r_0$  of 4.6 cm at the assumed imaging wavelength of 800 nm. The isoplanatic angle for the modeled atmosphere is 14  $\mu$  rad, a factor of 30 smaller than the FOV. The distorted scene fully illuminates a  $5 \times 5$  Shack-Hartmann lenslet array, which produces 25 images

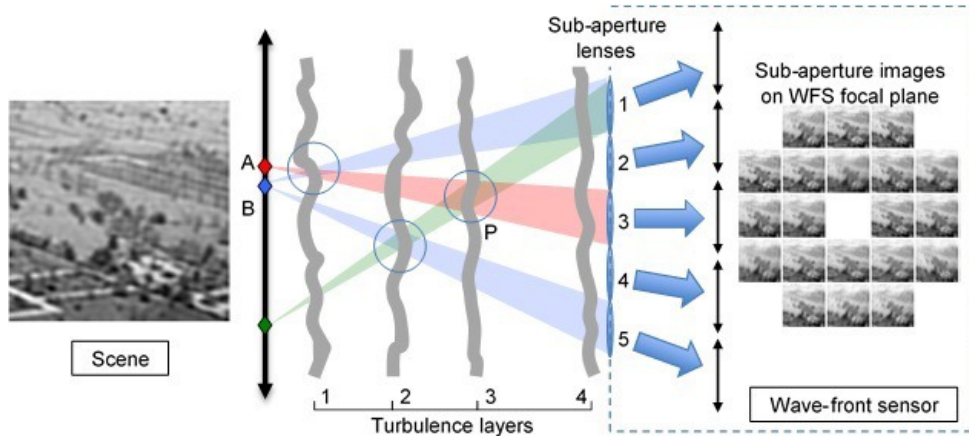


Figure 1. Cartoon of how tomography is enabled using an imaging Shack-Hartmann sensor. At any given time there are multiple field points that sample the same region of turbulence (for example, region P in layer 3 is sampled by field points A in the image from sub-aperture lens #3 and C in the image from sub-aperture lens #1)

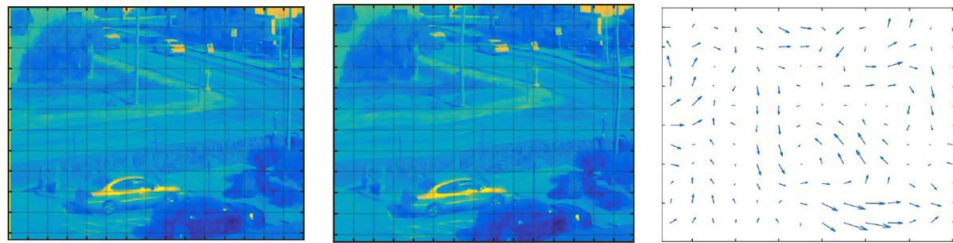


Figure 2. (Left) Pristine image. (Center) Artificially warped image. (Right) Warp map relating the images, represented as a quiver plot showing the local image deformation.

of the scene. We simulated 100 independent realizations, sampled at a pixel scale of  $4 \mu\text{rad}$ . To simulate the correction, the tomographic reconstruction of the aberrations was subtracted from the true aberrations. The result is illustrated in Figure 3 which shows a comparison of one of the aberrated images with the corresponding image after correction. There is a significant improvement in the fidelity of the corrected image: the resolution is essentially diffraction limited. We found that the PSF, averaged over all realizations, is corrected to the diffraction limit over the full FOV, with a constant Strehl ratio over most of the field as shown in Figure 4.



Figure 3. Examples of the simulated full-aperture images. With uncorrected atmospheric aberration (a); after correction (b). The on-axis PSFs for the two images are shown in (c) and (d), with different gray scales and expanded by a factor of four compared to the images. For reference, the size of the isoplanatic patch is shown on the left.

We seek to experimentally validate this technique through the development of a wide-field imaging Shack-Hartmann test bed. The work is being carried out as part of an overall research program that includes devel-

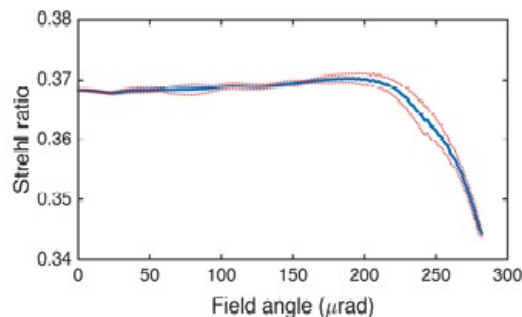


Figure 4. Long-exposure Strehl ratio of the compensated PSF as a function of field angle, averaged azimuthally, calculated for a wavelength of 800 nm. The dotted lines represent 1 standard deviation in our simulation of 100 instances.

opment of composite material optical systems (including deformable mirrors) and non-linear image restoration algorithms.<sup>5</sup> The end goal is to develop a family of robust, lightweight imaging systems that uses the wide-field tomographic wave-front sensing and nontraditional deformable mirrors to deliver high resolution imaging for aerospace applications.

## 2. SYSTEM DESIGN

The top-level logical flow of the optical system is described in Figure 5 which shows the major subsystems. To provide an accurate simulation we place requirements on the design of each of the subsystems. The first element is the scene generator which must deliver incoherent light to the turbulence simulator, and must be flexible enough that scenes with varying contrast and spatial frequency content can be projected. The scene generator contains an auto-focusing instrument that ensures best focus is maintained on the final imaging camera. For our generator we choose a digital LED screen with a pixel size small enough to be unresolved by our system. The second element is the turbulence simulator which imparts phase errors onto the wave-fronts from the scene generator. We require that the turbulence simulator be able to accurately simulate Kolmogorov turbulence over a range of spatial and temporal coherence scales,  $r_0$  and  $\tau_0$ . The light from the turbulence simulator is then imaged through the two arms of the down-stream optics. A 50/50 beam splitter sends half the light to the Shack-Hartmann wave-front sensor. The rest is sent to the imaging arm which consists of a single imaging lens that matches the  $F_{\#}$  and 0.5 degree FOV of the Shack-Hartmann arm. The imaging arm provides the reference image for the wave-front sensing, as well as the final image for the reconstruction. Figure 6 is an image of the built system and its components.

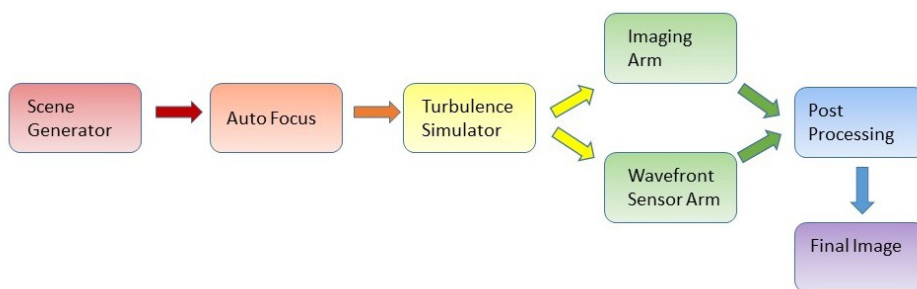


Figure 5. Flow chart of the operation of the test bed.

### 2.1 Scene Generator Design

The scene generator provides an incoherent object for the system. A LED computer screen of pixel size  $272 \mu\text{m}$  provides a  $500 \times 500$  pixel scene. The pixels are not resolved by our system. The light is propagated 2 m to a 200 mm focal length lens that is mounted on a motorized translation stage. A flip mirror may be inserted into the

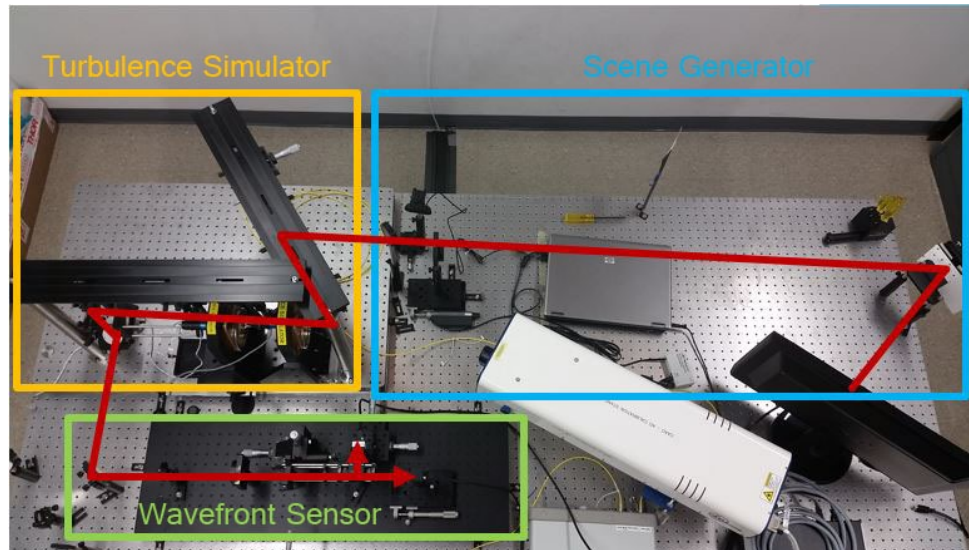


Figure 6. Photo of the testbed.

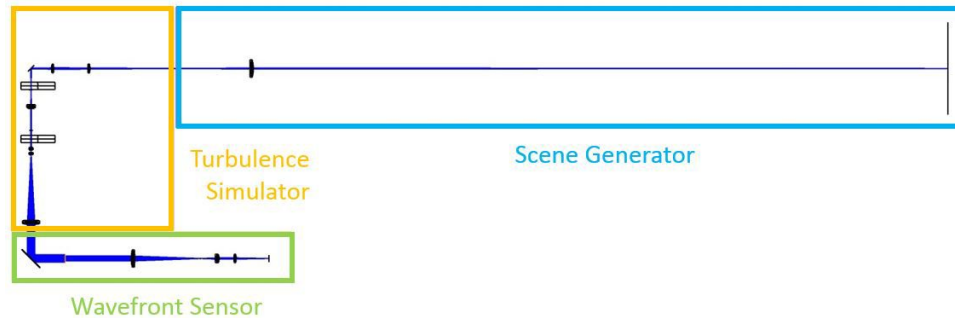


Figure 7. Zemax design of the testbed. Not shown is the beam splitter and lenslet array arm.

beam to feed an inexpensive webcam which serves as the focus reference for the system. A MATLAB algorithm reads the webcam and adjusts the lens to find the location of best focus, relying on a 3D integral of the MTF as the focus figure of merit. After focusing, the lens position is fixed and the flip mirror is removed to pass the scene into the turbulence simulator.

## 2.2 Turbulence Simulator

The turbulence simulator consists of two phase wheels. One is conjugated to the pupil of the system to simulate boundary layer turbulence. The second is placed in a converging beam to conjugate to a more distant atmospheric layer. This phase plate can be moved longitudinally to simulate different levels of  $D/r_0$ , and conjugate to different distances, although the two quantities cannot be adjusted independently. Figure 8 details the design of the turbulence simulator. A 14.75 mm object, delivered by the scene generator, is relayed through the first phase plate, placed near the intermediate image plane. This plate has an  $r_0$  value of 0.165 mm and in its nominal design position is conjugated 89 m from the pupil. The beam is then collimated, and a phase wheel of  $r_0 = 0.098$  mm is placed at the intermediate pupil plane. The combination of the two phase plates gives the system a total  $r_0$  of 1.209 mm. After the second phase plate, the light passes through a telescope which expands the beam to the desired pupil size of 21.2 mm for the wave-front sensor and imaging arms.

## 2.3 Wavefront Sensor Design

A first order, diffraction limited geometrical optics design of the imaging Shack-Hartmann testbed was produced and verified in Zemax. The system was designed to have a high Strehl of 90% or greater over the FOV. The

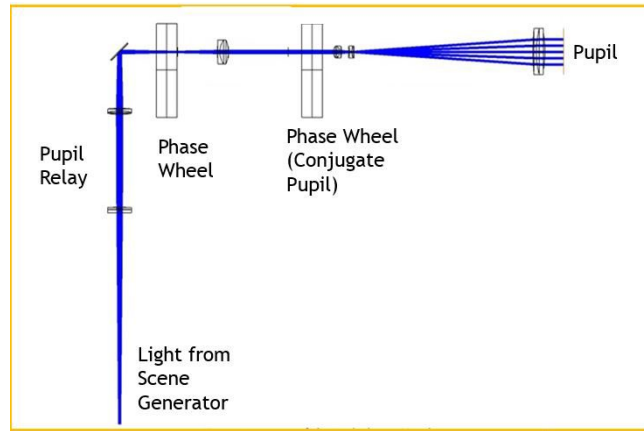


Figure 8. Layout of the Turbulence Simulator

design assures Nyquist sampling of the image by the detector pixels at a wavelength of 633 nm, and was then built using available stock parts from ThorLabs, with focal lengths picked to reduce the aberrations in the PSF to an acceptable level.

The pupil from the turbulence simulator is relayed through a  $4\times$  Keplerian relay consisting of 200 mm and 50 mm lenses. A beam splitter separates the light into two paths for the imaging and the WFS arms. These both have the same working focal ratio of 19 and a 0.5 degree field of view. Since the cameras used in the two arms are the same model with identical physical pixel size, this assures that the angular sampling, in units of the diffraction width, is the same. The WFS arm is built around a custom  $5 \times 5$  lenslet array of  $750 \mu\text{m}$  pitch, placed at a relayed pupil plane, and imaging onto a Point Grey Flea3 monochromatic sCMOS camera. The imaging arm consists of a single 100 mm imaging lens which focuses the image from the full aperture onto a second Flea3 camera. A field stop of diameter 2.5 mm is placed at the shared focal point of the  $4\times$  relay so that angular spread of the object is limited to the size of the detectors. The cameras have  $2.5 \mu\text{m}$  pixels and a detector size of  $5.2 \times 3.88 \text{ mm}$ . The final design of the imaging arm is illustrated in Figure 9.

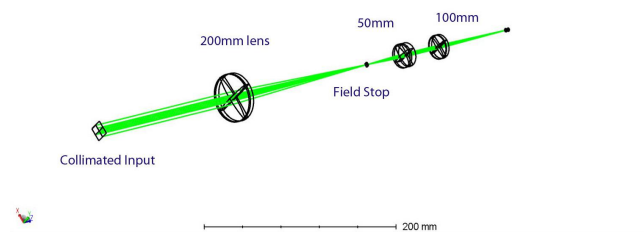


Figure 9. Zemax design of the imaging arm.

### 3. IMAGE POST PROCESSING

We seek to experimentally demonstrate that 3D tomographic reconstruction of atmospheric turbulence can be enabled by a novel application of a Shack-Hartmann lenslet array. The post processing of the data is as important as the test bed. The test bed will provide the necessary data, and the reduction pipeline will perform the tomosynthesis and produce a reconstructed image.

To generate the warp maps each sub-aperture image is divided into subsections and each subsection cross-correlated against a reference image. The highest spatial frequency information in the images defines the precision with which the local wave-front slopes may be estimated. The reference image is a running average in space and time of all the WFS sub-aperture images, with the time scale of the average chosen to correspond to an average flat wave front. The result is a single gradient vector for each image subsection that is a representation of the

relative distortions between the two. The size of the subsection is currently arbitrary, but should be set to the size of the isoplanatic angle on a real system.

Each warp map vector is the sum of tilts imparted by layers of atmospheric turbulence along the line of sight. Tomographic analysis of the tilt measurements along these line of sight path integrals allows us to estimate a 3D model of the aberrations.<sup>4</sup> The relationship between the measured data and the aberrations at the various layers of turbulence can be modeled as a linear inverse problem. If we assume the atmosphere is divided into a number  $L$  of discrete phase layers, and that each layer is discretized onto a grid with  $P$  elements, then the measured  $x, y$  slopes in sub-aperture  $i$ , image region  $j$ , are given by

$$\bar{\phi}_x(i, j) = \sum_{l=1}^L \sum_{k=1}^P w(i, j, k, l) \phi_x(j, l) + n_x(i, j) \quad (1)$$

$$\bar{\phi}_y(i, j) = \sum_{l=1}^L \sum_{k=1}^P w(i, j, k, l) \phi_y(j, l) + n_y(i, j) \quad (2)$$

where  $\phi_x$  and  $\phi_y$  are the actual wave-front gradients in the  $x$  and  $y$  directions,  $w$  is a window function that maps the footprint of sub-aperture  $i$  onto layer  $l$  along the line-of-sight  $j$  and  $n$  represents the unknown noise. We seek a solution to  $\Phi = R\phi$ , where  $\Phi$  is the set of wavefront phases on the  $L$  layers,  $\phi$  is a vector of all the measured phase gradients, and  $R$  is the “reconstruction” matrix that relates them, i.e.

$$\begin{bmatrix} \phi_1 \\ \vdots \\ \vdots \\ \phi_L \end{bmatrix} = R \begin{bmatrix} \bar{\phi}_x \\ \vdots \\ \bar{\phi}_y \\ \vdots \end{bmatrix} \quad (3)$$

The matrix  $R$  is found by inverting the measured effect of a set of basis functions on the WFS signals. For simplicity in the simulations described below, we chose Fourier modes defined on a square grid, supplemented with tip and tilt. The effect of each mode on the WFS signal  $\phi$  is calculated, and the results compiled into an influence matrix  $F$  such that  $\phi = F\Phi$ . We then find  $R$  as the pseudo-inverse of  $F$  using a truncated singular value decomposition (SVD).

#### 4. RESULTS

Final results are still in progress. The alignment of the testbed is finished and we have successfully imaged a scene through the system. We are currently on the stage of generating warp maps. Figure 10 is an example of a warp map generated from a sub-aperture image (middle) compared to a reference (left). The reference was created using a running average of 50 frames of the same subaperture image. In the final iteration of this experiment, the reference image will be a running average from the full aperture imaging arm. For our final results we expect a grid of warp maps as shown in Figure 11. Each warp map corresponds to a single sub-aperture scene. Applying a reconstruction matrix to a vector constructed from all the warp map gradients will return a vector of wave-front phases corresponding to atmospheric layers at predefined ranges corresponding to the two phase plates in the turbulence simulator.

#### 5. FUTURE WORK

Future work will see the warp map analysis finished. After a grid of warp maps is completed, we will perform the tomographic analysis to generate wave-front phases in discrete layers corresponding to the phase plates. We will then compute PSFs along lines of sight through the modeled atmosphere with a density that matches the angular size of the isoplanatic field, and deconvolve them from the full-aperture image using iterative estimation techniques.<sup>5</sup> In parallel we will continue to investigate non-traditional deformable mirror substrates. The final system will use a reconstruction matrix calculated by the tomographic analysis to drive a single deformable mirror placed in the pupil. This will remove the isoplanatic component of the aberration common to all points in the field. Residual field-dependent terms will be removed using the numerical approach.

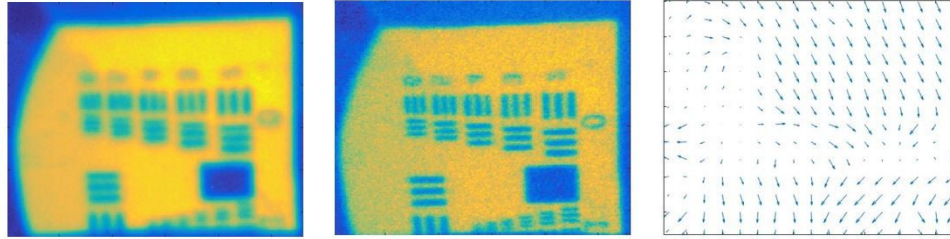


Figure 10. (Left) Running average made from 50 averaged lenslet frames. (Middle) Single lenslet image. (Right) Warp map generated from the autocorrelation of the subregions from the two images.

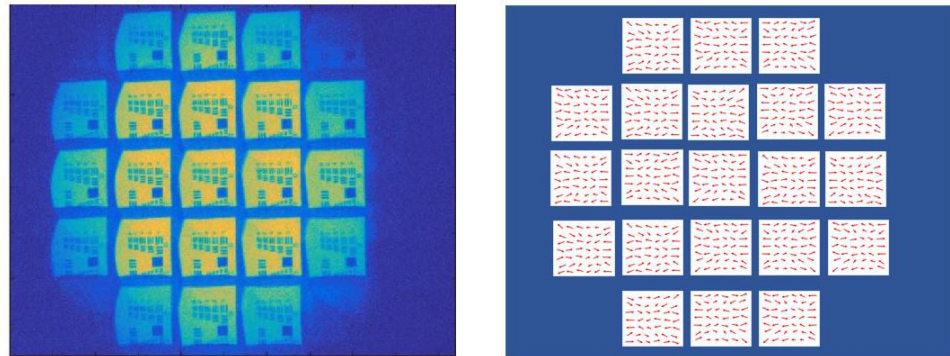


Figure 11. (Left) Images of the scene through each sub-aperture. (Right) Grid of simulated warp maps of each corresponding sub-aperture image, illustrating the geometric relationship between the warp maps, representing our estimates of the wave-front gradients, and the WFS data.

## ACKNOWLEDGMENTS

This work has been funded by the Office of Research and Discovery and the College of Optical Sciences at The University of Arizona.

## REFERENCES

1. G. Moretto, M. Langlois, P. Goode, N. Gorceix and S. Shumko, "Design for solar multi-conjugate adaptive optics at the New Solar Telescope/Big Bear solar observatory," in *Adaptive Optics for Extremely Large Telescopes*, Third AO4ELT Conference, Florence, Italy (2013).
2. T. Rimmele, S. Hegwer, K. Richards, F. Wger, J. Marino, D. Schmidt, and T. Waldmann, "Solar multiconjugate adaptive optics at the Dunn Solar Telescope," *Proceedings of the Advanced Maui Optical and Space Surveillance Technologies Conference*, held in Wailea, Maui, Hawaii, September 16-19, 2008, Ed.: S. Ryan, The Maui Economic Development Board, p. E18 (2008).
3. J. M. Trujillo-Sevilla, L. F. Rodriguez-Ramos, J. J. Fernandez-Valdivia, J. G. Marichal-Hernandez and J. M. Rodriguez-Ramos, "Tomographic wavefront retrieval by combined use of geometric and plenoptic sensors," in *Optical Sensing and Detection III (Proc. SPIE)*, eds. Berghmans, F., Mignani, A. G., & De Moor, P., 9141, 914129 (2014).
4. J. M. Beckers, "Multiconjugate adaptive optics: experiments in atmospheric tomography," in *Adaptive Optical Systems Technology (Proc. SPIE)* ed. Wizinowich, P. L., 4007, 466–475 (2000).
5. D.A. Hope, M. Hart, S.M. Jefferies and J. Nagy, "Robust image restoration for ground-based space surveillance," in *Proceedings of the Advanced Maui Optical and Space Surveillance Technologies Conference*, held in Wailea, Maui, Hawaii, 2013, Ed.: S. Ryan.